Acta Geophysica (2018) 66:461–477
https://doi.org/10.1007/s11600-018-0140-3

RESEARCH ARTICLE - SOLID EARTH SCIENCES

Modeling of the strong ground motion of 25th April 2015 Nepal earthquake using modified semi-empirical technique

Sohan Lal[1] · A. Joshi[1] · Sandeep[2] · Monu Tomer[3] · Parveen Kumar[4] · Chun-Hsiang Kuo[5] · Che-Min Lin[6] · Kuo-Liang Wen[7] · M. L. Sharma[7]

Received: 30 September 2017 / Accepted: 4 April 2018 / Published online: 18 May 2018

Abstract
On 25th April, 2015 a hazardous earthquake of moment magnitude 7.9 occurred in Nepal. Accelerographs were used to record the Nepal earthquake which is installed in the Kumaon region in the Himalayan state of Uttrakhand. The distance of the recorded stations in the Kumaon region from the epicenter of the earthquake is about 420–515 km. Modified semi-empirical technique of modeling finite faults has been used in this paper to simulate strong earthquake at these stations. Source parameters of the Nepal aftershock have been also calculated using the Brune model in the present study which are used in the modeling of the Nepal main shock. The obtained value of the seismic moment and stress drop is 8.26×10^{25} dyn cm and 10.48 bar, respectively, for the aftershock from the Brune model .The simulated earthquake time series were compared with the observed records of the earthquake. The comparison of full waveform and its response spectra has been made to finalize the rupture parameters and its location. The rupture of the earthquake was propagated in the NE–SW direction from the hypocenter with the rupture velocity 3.0 km/s from a distance of 80 km from Kathmandu in NW direction at a depth of 12 km as per compared results.

Keywords Strong motion · Himalayan seismicity · Displacement spectra · Response spectra · Site amplification · Modeling

Introduction

A major earthquake occurred in the central seismic gap of the Himalaya in Nepal of magnitude 7.9 (M_w) on 25 April, 2015. More than 8000 people were killed by the earthquake. Economic losses were estimated to be around $ 3.5 billion (CEDIM). It is estimated that total damage is caused by the short period strong motion due to any earthquake. Civil engineers use these ground motions which contain high frequency provide key parameters which are used for safe design and. Source characteristics of the earthquake are also illustrated by the high-frequency strong ground motion. All the sites did not feel the strong motion in past, due to this only modeling of high frequency strong ground motion (SGM) is left. This lack of data causes a big issue in calculating the parameters which are very important in designing the earthquake-resistant buildings. To design the safe building at such sites, simulation of the strong motion is preferred. SGM can be simulated using several techniques which include Stochastic Modeling of the strong

✉ Sohan Lal
sohangeokuk@gmail.com

[1] Department of Earth Sciences, Indian Institute of Technology Roorkee, Roorkee, India

[2] Department of Geophysics, Institute of Science, Banaras Hindu University, Varanasi, India

[3] Geological Survey of India, Hyderabad, India

[4] Wadia Institute of Himalayan Geology, Dehradun, India

[5] National Centre for Research on Earthquake Engineering, Taipei, Taiwan

[6] Department of Earth Sciences, National Central University, Chungli, Taiwan

[7] Department of Earthquake Engineering, Indian Institute of Technology Roorkee, Roorkee, India

motion data based on the random theory technique, Composite Source Modeling technique, etc. and Empirical Green Function methodology based on the uses of the foreshock or aftershock as Green function of the small segments of the main shock rupture.

Stochastic method was suggested by the engineers whose major objective was to predict the hazard result for designing purpose. The Stochastic technique was initially given by Housner and Jennings (1964). This method made use of previously provided database for simulating ground motion at any site. It starts with making use of a random noise built in time series, then it transforms it into the frequency domain and replaces the amplitude spectrum of the noise with the desired spectrum speculated at the region under consideration. One does not alter the phase part as it may then distort the signal to unrecovered extent. Then, it is passed through a time window which is founded on the basis of our older records; the window is built in accordance with the variation found in the older records and the final transient signal in the time domain is considered to be the modeled result for the strong ground motion (Boore 1983). It works well for point source model but fails for other realistic sources. It does not incorporate the parameters related to the source and the propagation of the earthquake. It is purely statistical in nature and works only for designing purposes.

It taps the properties of random Gaussian noise to create a signal that is non-stationary in nature which resembles to some extent to the seismic earthquake record in that region (Atkinson and Boore 1995, 1998; Boore 1983; Boore and Joyner 1991; Hanks and McGuire 1981; Housner and Jennings 1964; McGuire et al. 1984; Sinozuka and Sato 1967; Lai 1982; Beresnev and Atkinson 1997, 1999). Atkinson and Boore (2006) developed the prediction equations for the ground motion of the rock and soil sites using the stochastic method. Rigan earthquake occurred in 2010 has been modeled using the Stochastic method (Safarshahi et al. 2013).

Empirical Green Function technique was initiated by Hartzell (1978). This methodology is powerful tool for the modeling of the SGM due to an earthquake. To model the large earthquake by this technique, it requires the aftershock or foreshock as Green function from the same location where the main shock occurred. This technique is further used and modified to model the large earthquake by Imagawa et al. (1984), Heaton and Hartzell (1989), Hadley et al. (1982), Haddon (1996), Irikura (1983), Houston and Kanamori (1984), Munguia and Brune (1984), Hutchings (1985), Kanamori (1979), Hartzell (1982), and Kohrs-Sansorny et al. (2005). The main advantage of the technique is that it does not need site correction (Fukuyama and Irikura 1986). However, it is found that modeling of the SGM due to an earthquake using the Empirical Green Function is also used to model the broadband data. However, aftershock or foreshock at each modeling site is not available to be used as Green function and the technique requires the detailed knowledge of the source rupture.

A Composite Source Model, incorporating different sized sub-events, provides a possible description of complex rupture processes during earthquakes (Yu 1994; Zeng et al. 1994; Yu et al. 1995). This technique considers the complex source mechanism of the earthquake for computing realistic synthetic strong-motion seismograms using synthetic Green's function (Khattri et al. 1994). The technique considers that the source is composed of a randomly distributed circular sub-events having constant stress drop. The power-law distribution is followed by all the sub-events and their radius (Frankel 1991).The main disadvantage of the technique is that it requires the complete source mechanism of the earthquake which is used in computing the theoretical Green's function. This requirement is not easily available and hence reliability of final simulation is always questionable.

Semi-empirical technique is one of the techniques which considers the advantage of the stochastic simulation technique and Empirical Green's Function technique. The semi-empirical method was proposed by Midorikawa (1993) and further modified by Joshi and Midorikawa (2004). In this method, simulated time series from various sub-faults are used as Green's function instead of aftershock records. The technique is very fast to calculate the modeling parameters as it is dependent on attenuation relation. Various earthquakes have been simulated using this technique. The applicability and importance of this technique have been validated by simulating records of various earthquakes like the 2011 Tohuku earthquake and the 2004 Sumatra. Several modifications have been done in the technique which includes the addition of layered earth model, addition of entire time series in acceleration (Joshi et al. 2001), correction factor (Joshi and Midorikawa 2004), envelop function with scaling of seismic moment (Joshi et al. 2001), addition of radiation pattern (Joshi et al. 2012a), component wise simulation of acceleration record (Joshi et al. 2012b) and addition of strong motion generation areas (Joshi et al. 2014). In the present paper, modified semi-empirical technique (MSET) has been used for simulation of SGM which includes all modification done in semi-empirical technique by Joshi and Patel (1997) and Joshi et al. (1999, 2001, 2012a, b, 2014).

Epicenter of the Nepal earthquake was located at a distance of around 420 to 515 km from the network of recording stations in the Kumaon Himalaya. The data from Kantipath station, which is near Kathmandu and is at a distance of 59 km from the epicenter of the earthquake, are available for the present study provided by the United States Geological Survey (USGS). The main purpose of

this study is to finalize the model parameters of the Nepal earthquake using strong motion data recorded at several stations. The main objective of this work is to model the main shock Nepal earthquake using the aftershock and calculating the source parameters of the aftershock which are used in modeling the main shock of the Nepal earthquake. The technique used in the present work is component wise simulation of the strong motion data (Joshi et al. 2012b).

Geology and tectonics

The expanse of the Himalaya is 2400 km long and 300–400 km wide. The Himalayan province is divided into mainly four physiographic domains which are distinguished based on the rock type, their ages and geomorphology. The four domains from southern side to the northern side are (a) Shiwalik Himalaya (b) Lesser Himalaya (c) Higher Himalaya (d) Tethys Himalaya as shown in Fig. 1. The Kumaon–Garhwal region of the Himalaya is situated in the middle of the Himalayan folded-and-thrust belt. The central Himalaya has 2500–3000 m high and remarked by rounded hilltop, gentel slopes and undulating landscape. Most of the seismic activity occurred in the lesser Himalaya. Lesser Himalaya is separated by Main Boundary Thrust from Shiwalik Himalaya in the south and in the north separated from the Great Himalaya by Main Central Thrust. Tehyths Himalaya consists of sedimentary and Meta sedimentary rocks with low grade metamorphic (Yin 2006). Greater Himalaya mostly consists of high-grade crystalline rock with migmatites South Tibet Detachment at top and Main Central Thrust at bottom. Lesser Himalaya thrusting over Shiwalik Himalaya along Main Boundary Thrust, which mainly consists of meta-sediments with high-grade crystal lines in form of Nappe and Klippe. Sub-Himalaya mainly consists of sedimentary rocks with well-preserved fossils representing a low degree of metamorphism.

After occurring the Nepal earthquake, it has been observed that seismicity moved towards eastern side of the epicenter of the Nepal earthquake as shown in Fig. 1.

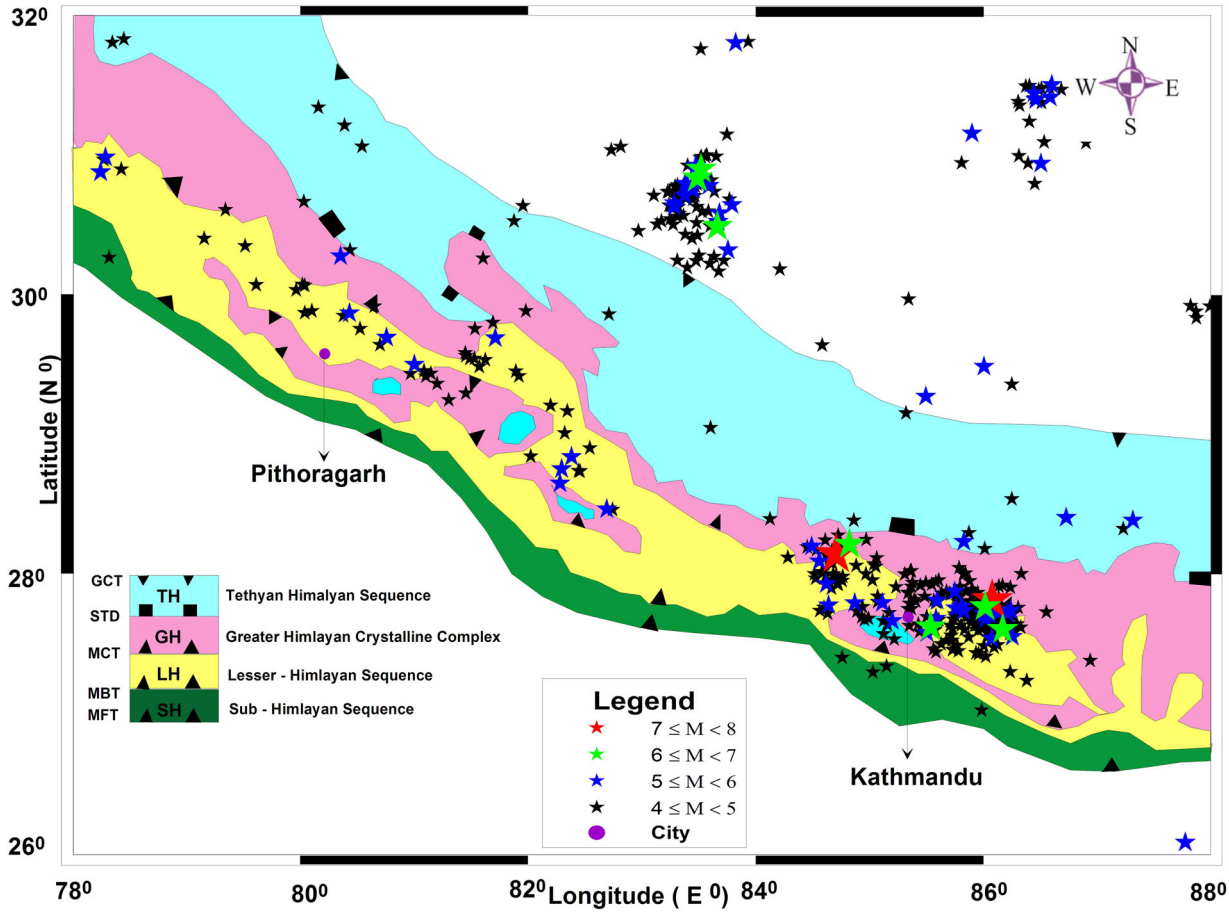

Fig. 1 Tectonic map of the Himalayan region (Yin 2006). Seismicity before and after the Nepal earthquake 25 April 2015. Red star shows the epicenter of the Nepal earthquake

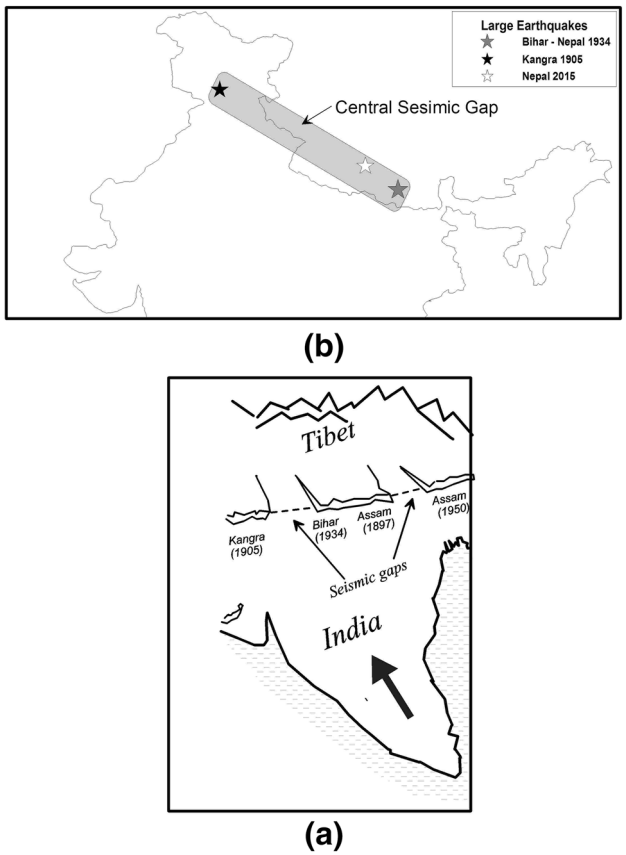

Fig. 2 **a** Seismic gaps suggested in Indian Himalayan region. **b** Central seismic gap region between the Bihar earthquake and Kangra earthquake given by Khatrri (1987)

Nepal earthquake lies in this area of the central seismic gap (Khattri 1987) as shown in Fig. 2.

Data

Source parameters of the Gorkha Nepal earthquake are given in Table 1. Accelerograph installed in the Kumaon Himalaya record the Nepal earthquake .The epicentral distance of the stations is between 420 and 515 km. Three-component force balanced high-frequency Kinemetrics' ETNA accelerograph is installed at each station. The response of the instrument is flat up to 50 Hz. The threshold of these accelerometers is 0.005% of full scale and sensitivity of the accelerometer is 1.25 V/g. The processing of the recorded data is done using the Boore and Bommer (2005) procedure. Strong motion record from near field station at Kantipath is also available for the study (USGS). This station lies at a distance of 59 km from the epicenter of this earthquake. Peak ground acceleration (PGA) at this station is 187 gals which is supposedly low, keeping in view the damage caused by this earthquake. The hypocentral parameters of this earthquake are shown in Table 1.

Accelerographs are placed in the Government schools which have site effects due to which energy gets amplified. We have calculated site effects using the technique of *H*/*V* spectral ratio method which is initially given by Nakamura (1989). The North–South component of accelerogram for the Nepal earthquake after applying the site correction is shown in Fig. 3. The time series of the Kumaon array are processed using Butterworth filter with the range of 0.01–25 HZ. Butterworth band-pass filter has been applied ranging from 0.4 to 25 Hz, to remove the low-frequency component from the accelerogram records at Kantipath station. The processed N–S and E–W components of the Nepal earthquake recorded at Kantipath station are shown in Fig. 4.

Methodology

Component wise simulation of strong ground motion given by Joshi et al. (2012b) has been used in the present study. The amplitude spectrum of white Gaussian noise with zero expected mean and unit spectral amplitude is used to obtained acceleration spectrum of the target earthquake which is further transformed into time series using appropriate signal processing tools in the technique. This spectrum of noise has been passed through various filters and constants which are defined by Boore (1983) as follows:

$$A(f,R) = C \cdot S(f) \cdot D_{\mathrm{s}}(f) \cdot F_{\mathrm{R}}(f,R) \quad (1)$$

In Eq. (1) C and other filters are defined as:

$$C = M_0 \cdot R_{\theta\varphi} \cdot \mathrm{FS} \cdot \mathrm{PRTITN} / 4\pi\rho\beta^3 \quad (2)$$

$$S(f) = (2\pi f)^2 \Big/ \left[1 + (f/f_{\mathrm{c}})^2\right] \quad (3)$$

$$D_{\mathrm{S}}(f) = 1 \Big/ \left[1 + (f/f_{\mathrm{m}})^8\right]^{1/2} \quad (4)$$

Table 1 Fault plane parameters of Nepal earthquake

Origin time	Location	Size	Fault plane solution	Agency
25/04/15	28.15°N, 84.71°E	M_{w}= 7.8	NP1 Φ = 295°, δ = 11°, λ = 108°	USGS
6:11:26.27	Depth = 10 km	$M_{\mathrm{o}} = 5.45 \times 10^{27}$ dyn cm	NP2 Φ = 99°, δ = 83°, λ = 89°	
25/04/15	27.77°N, 85.37°E	M_{w} = 7.9	NP1 Φ = 287°, δ = 6°, λ = 108°	Global Centroid Moment Tensor (CMT)
6:11:58.4	Depth = 12 km	$M_{\mathrm{o}} = 7.76 \times 10^{27}$ dyn cm	NP2 Φ = 101°, δ = 84°, λ = 89°	
		M_{s} = 7.9		

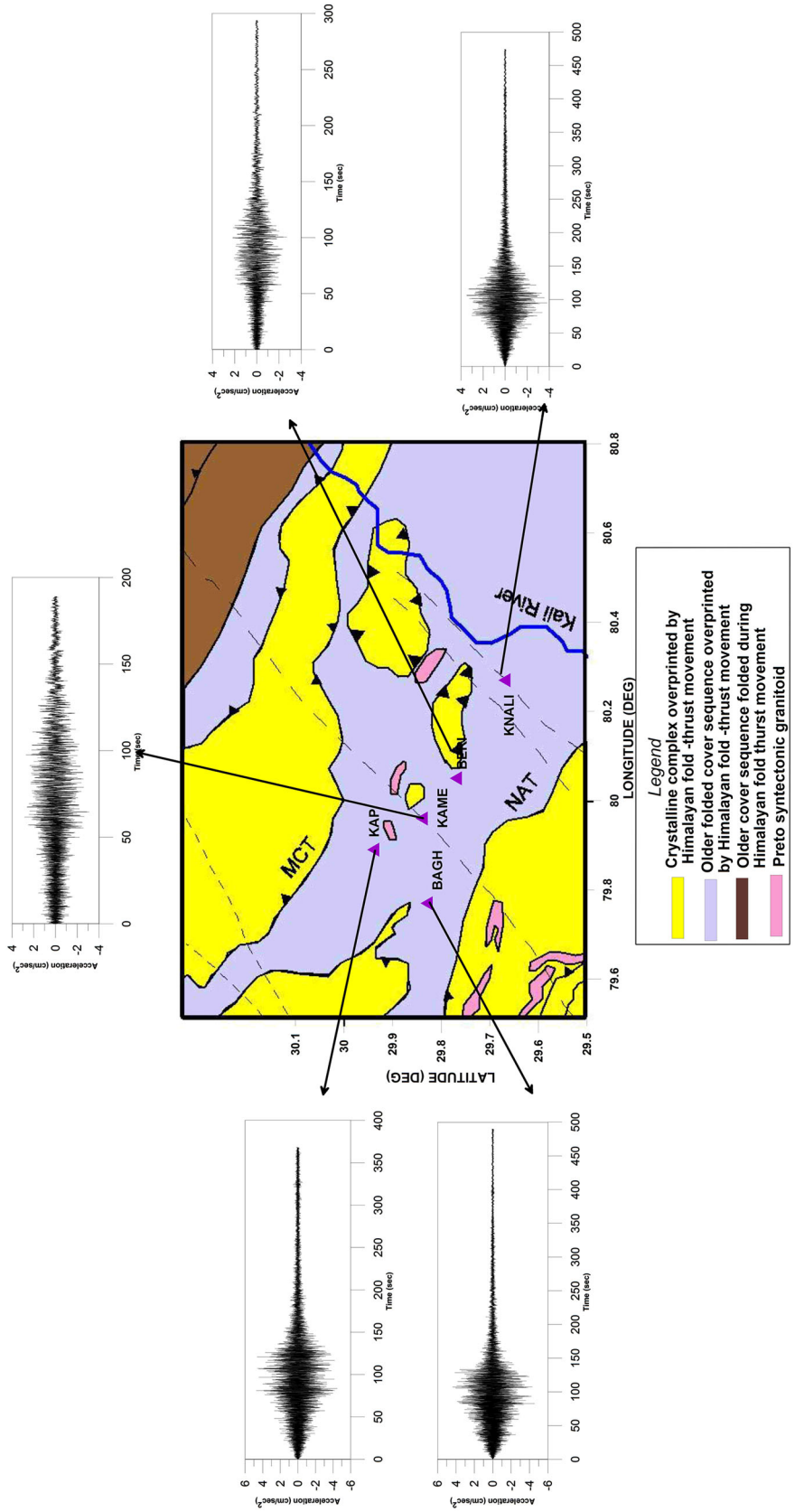

Fig. 3 Corrected NS accelerograms at rock site at different station of Kumaon array

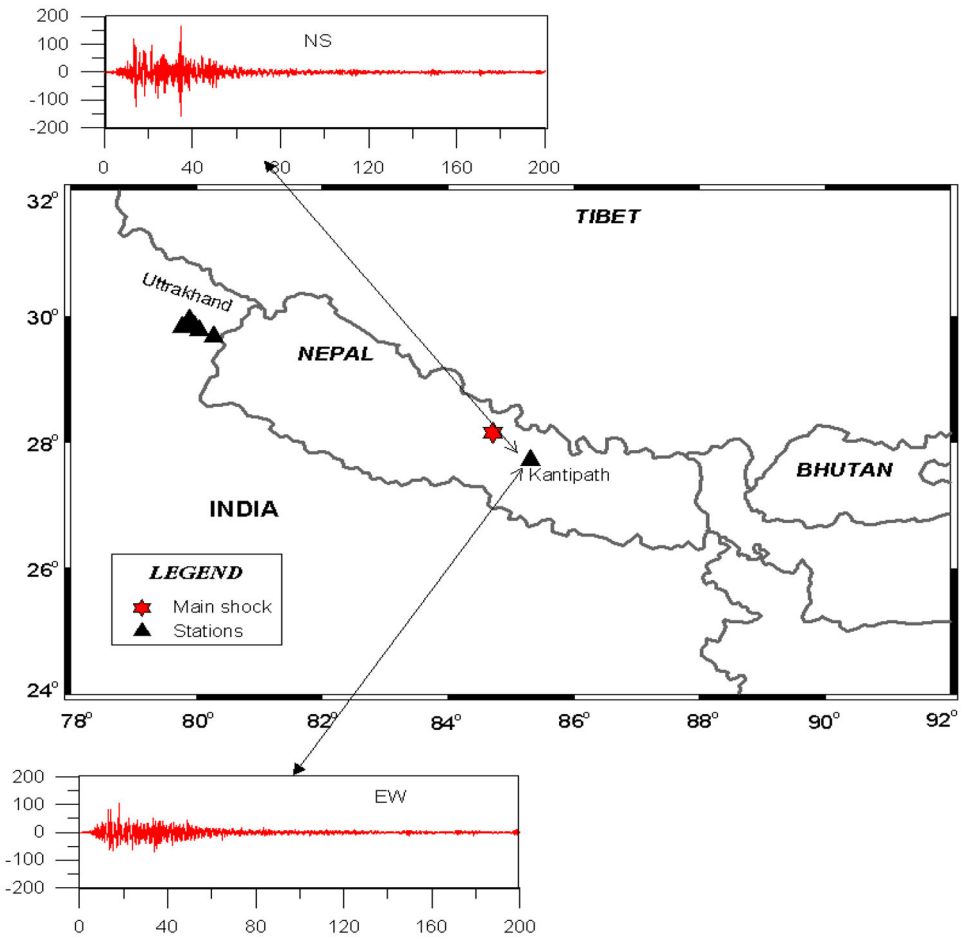

Fig. 4 Processed accelerograms at near field station Kantipath (USGS)

$$F_{\mathrm{R}}(f,R) = \left(e^{-\pi fR/\beta Q_{\beta}(f)}\right)\Big/R \tag{5}$$

In Eq. (2), seismic moment is represented by M_{o}; β and ρ are the shear wave velocity and the density of the medium, respectively; $R_{\theta\varphi}$ is radiation pattern which is affected by rupture parameters; amplification caused by the free surface of the site is represented by FS, PRTITN defines the splitting of energy of the SH wave (taken as $1/\sqrt{2}$). The filter $S(f)$ in Eq. (1) represents the acceleration spectrum of source (Brune 1970); Boore (1983) gives the formulae for the high-frequency attenuation and filter total anelastic attenuation which is represented by $D_{\mathrm{S}}(f)$ and $F_{\mathrm{R}}(f, R)$, respectively, in the Eq. (1). In the above expressions, R is the hypocentral distance and $Q_{\beta}(f)$ is the shear wave quality factor which depends on the frequency.

The theoretical filters used in Eq. (1) were multiplied with white Gaussian noise spectrum to obtain the earthquake acceleration spectra. The acceleration spectrum is further converted into acceleration time series which is represented by acceleration record '$a_{ij}(t)$' of earthquakes represented by sub-faults. Small and the target earthquake slips with different time duration, this difference in the slip duration cause a problem. This problem is compensated using the correction function $F(t)$, by convolving this with the acceleration record. This function is also used to overcome the problem of low-frequency mismatching and is given by Irikura and Kamae (1994) and Irikura et al. (1997).

$$F(t) = \delta(t) + [(N-1)/T_{\mathrm{R}}(1-\exp(-1))] \cdot \exp(-t/T_{\mathrm{R}}) \tag{6}$$

$$A_{ij}(t) = F(t) * a_{ij}(t) \tag{7}$$

In Eq. (7), subscripts i and j represent the location of sub-fault along the length and the width of the rupture plane, respectively. Kameda and Sugito (1978) provides the envelope function. This function act as window function which is used to get the acceleration record from the above equation; the function is modified by adding the term transmission coefficient of shear wave Joshi (2004):

$$e_{ij}(t) = T_{\mathrm{ss}}(t/T_{\mathrm{d}}) \cdot \exp(1 - t/T_{\mathrm{d}}) \tag{8}$$

In Eq. (8), T_{d} is the time duration and T_{ss} is the transmission coefficient of shear waves. We need to divide the target earthquake rupture into N^2 small earthquakes that are responsible for the target earthquake on the basis of self-similarities law of geometrical parameters. Acceleration

envelope is used in place of aftershocks in the present technique based on the empirical relations as empirical Green function. Kanamori and Anderson (1975) give the self-similarities geometrical relations between the target and small earthquakes that have been used to determine the number of sub-faults which gives the response to the target earthquake.

Nucleation point is one sub-fault from which the rupture starts propagating along the radius, which is decided after division of the rupture into various sub-faults. The energy is released by each sub-fault whenever the rupture front approaches its centre. The resultant acceleration record $ac_{ij}(t)$ is the product of acceleration record $A_{ij}(t)$ from filtered white Gaussian noise with the acceleration envelope function $e_{ij}(t)$. This is given as:

$$\mathrm{ac}_{ij}(t) = e_{ij}(t) \cdot A_{ij}(t) \tag{9}$$

The acceleration record $ac_{ij}(t)$ released from different ijth subfaults to be resolved into two components along the direction of strike and dip using the formula given by Joshi et al. (2012b).

$$\mathrm{ac}_{ij}^{X}(t) = \mathrm{ac}_{ij}(t) \cdot \cos\theta_{ij} \cdot \cos\varphi_{ij} \tag{10}$$

$$\mathrm{ac}_{ij}^{Y}(t) = \mathrm{ac}_{ij}(t) \cdot \cos\theta_{ij} \cdot \sin\varphi_{ij} \tag{11}$$

In Eqs. (10) and (11), $\mathrm{ac}_{ij}^{X}(t)$ and $\mathrm{ac}_{ij}^{Y}(t)$ represent the acceleration components along the strike and dip directions, respectively. The angle φ_{ij} and θ_{ij} used in Eqs. (10) and (11) are shown in Fig. 5. The obtained results are rotated by angle $\emptyset$ Joshi et al. (2012b).

$$\begin{bmatrix} \mathrm{ac}_{ij}^{\mathrm{NS}} \\ \mathrm{ac}_{ij}^{\mathrm{EW}} \end{bmatrix} = \begin{bmatrix} \cos\phi & -\sin\phi \\ \sin\phi & \cos\phi \end{bmatrix} \begin{bmatrix} \mathrm{ac}_{ij}^{X}(t) \\ \mathrm{ac}_{ij}^{Y}(t) \end{bmatrix} \tag{12}$$

Summing of all NS and ES component of records released from various sub-faults at various time lag 't_{ij}' gives the end result for the NS and EW components. This is represented by the following formula given by Joshi et al. (2012b):

$$\mathrm{Ac}^{\mathrm{NS}}(t) = \sum_{i=1}^{N}\sum_{j=1}^{N} \mathrm{ac}_{ij}^{\mathrm{NS}}(t - t_{ij}) \tag{13}$$

$$\mathrm{Ac}^{\mathrm{EW}}(t) = \sum_{i=1}^{N}\sum_{j=1}^{N} \mathrm{ac}_{ij}^{\mathrm{EW}}(t - t_{ij}). \tag{14}$$

Parameters of the target and sub-fault earthquake

In MSET of simulation, the faulted rupture of the supposed target earthquake is segmented into sub-faults using self-similarity laws. These laws have been given by Kanamori and Anderson (1975) and Aki (1967) as discussed in the above section. The application of these laws requires extensive knowledge of the source parameters of target and the sub-fault event. Corner frequency, stress drop and seismic moment are the source parameters which are obtained from source displacement spectra. In this study, the source parameters of the aftershocks of the Nepal earthquake are calculated from the accelerograms recorded at various stations which are situated in the Himalayan region of Uttrakhand State, India using the grid search algorithm. Displacement spectrum of source at five stations is calculated using the equation given by Brune (1970) for the aftershock. Comparison between the observed and theoretical displacement spectra is used to estimate corner frequency at which the spectra fall for the aftershock. This comparison is shown in Fig. 6 at stations of the Kumaon network. The source parameters such as stress drop, etc. which are listed in Table 3 of this earthquake from the accelergram at each of the five stations are calculated. The value of source parameters obtained from five different records of the main shock and aftershock is given in Table 3. Figure 6 shows the source displacement spectra of the aftershock recorded at stations of the Kumaon Himalayan network.

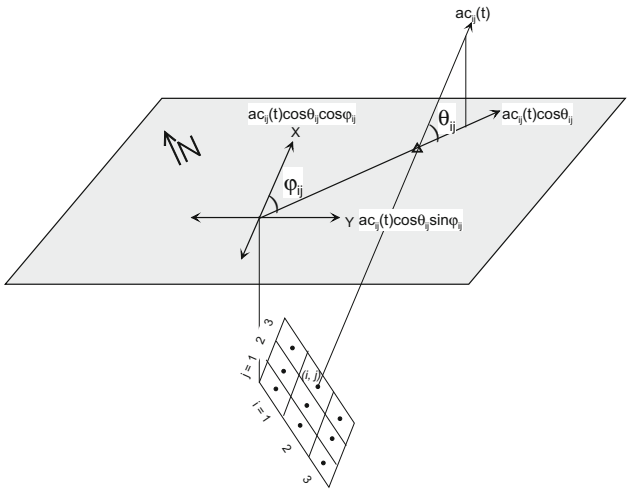

Fig. 5 Simulation of the acceleration record released by ij sub-fault along of the NS and EW component (after Joshi et al 2012b)

It is seen from Table 2 that the value of seismic moment obtained from displacement spectra of the Nepal earthquake and its aftershock is nearly equal to that obtained from USGS and CMT Harvard. The average value of the stress drop calculated for the Nepal earthquake and its aftershock is given in Table 2 which is within the reasonable range of stress drop calculated by different workers for Himalayan earthquake (Wason and Sharma 2000; Sriram and Khattri 1997; Kumar et al. 2005). The calculated parameters of the earthquake are within the

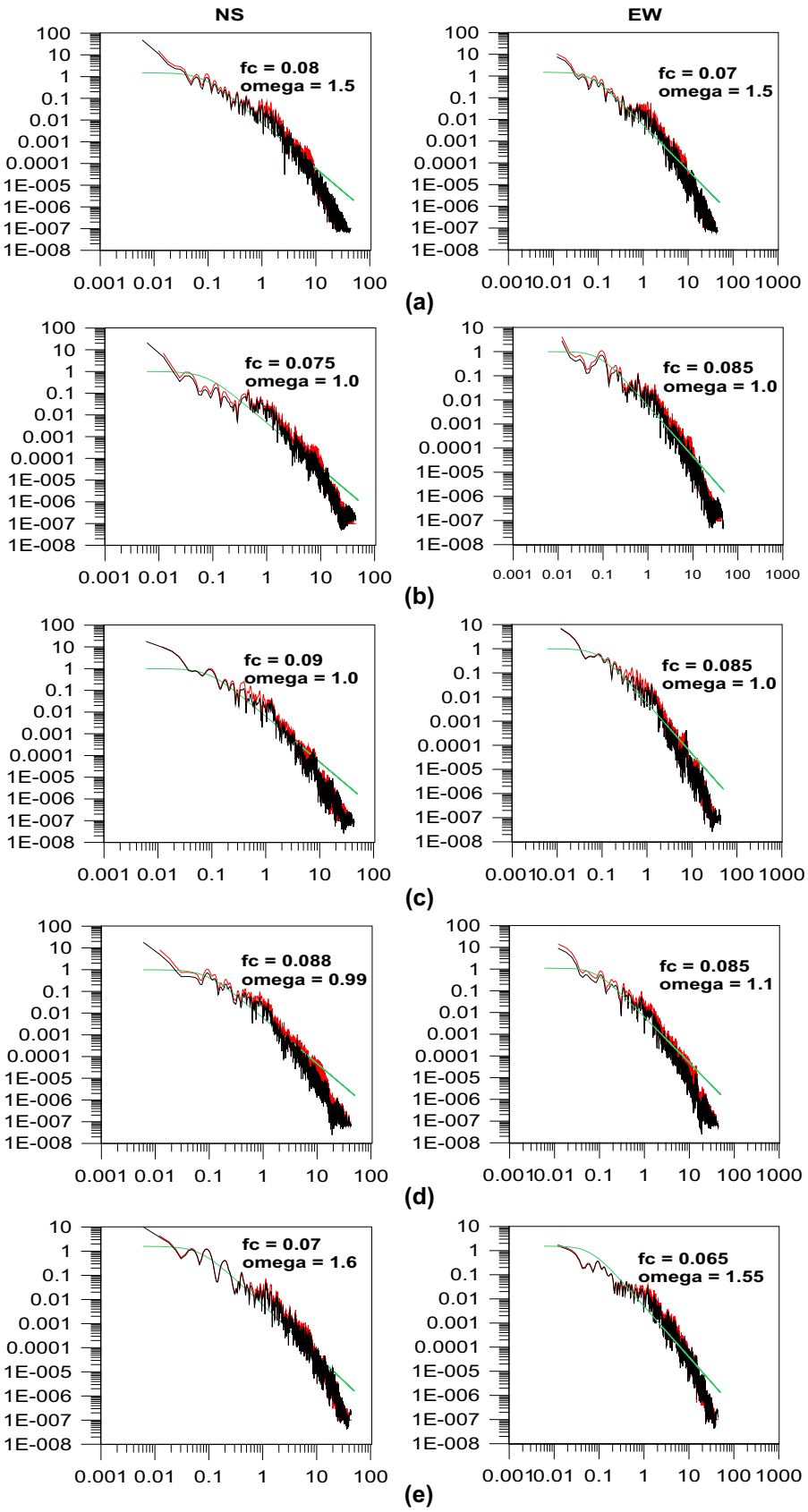

Fig. 6 Source displacement spectra for the aftershock at Kumaon stations **a** Knalichina, **b** Bageshwar, **c** Berinag, **d** Kamedidevi and **e** Kapkot, respectively, where red color shows the observed spectra at the soil site and black color shows the observed spectra at rock site and Green color shows the theoretical spectra

Table 2 Obtained source parameters of the Nepal earthquakes (a) main shock (Joshi et. al. 2016) and (b) aftershock (present study) using the Accelerograms

S. no.	Source parameters	Average ± standard deviation	
		Main shock	After shock
1	Corner frequency (f_c)	0.027 ± 0.002	0.07 ± 0.01
2	Seismic moment M_o (dyne-cm)	(3.53 ± 0.28) × 10^{27}	(8.26 ± 2.21) × 10^{25}
3	Source radius (km)	44.13 ± 3.85	15.16 ± 2
4	Stress drop (bar)	18.68 ± 5.93	10.48 ± 1.7
5	Moment magnitude (M_w)	7.7 ± 0.02	6.56 ± 0.05

acceptable range of value obtained for the Himalayan earthquake obtained by earlier studies. The length of the rupture and downward extension is calculated as 145 and 42 km, respectively, using the relations given by Wells and Coppersmith (1994). The area obtained by the empirical relation given by Wells and Coppersmith (1994) is 6090 km^2 which is close to that obtained as 5278 km^2 for circular rupture which is obtained using parameters obtained from source displacement spectra.

Model selections

It has been observed that the simulations of the earthquake are affected by various rupture parameters. Once the initial modeling parameters have been decided, next work was to find the parameters of the rupture plane. In the present work, model was selected on the basis of minimum root mean square error (RMSE) between the simulated and observed acceleration waveform at Kantipath station. The following formula for RMSE comparison has been used in the present work:

$$\mathrm{RMSE} = [(1/N) \cdot \Sigma(a(i) - b(i))/a(i))^2]^{1/2}$$

where $a(i)$ and $b(i)$ are observed and simulated accelerations records, respectively. The parameter N represents the total number of samples in record. It is observed that change in the parameters affects simulation of the strong motion records very much. Although guess of initial of the rupture parameters can be made using the previous studies or it may be independent studies. To final the model iterative modeling has been done and obtained results are compared with the observed data in terms of root mean square error. Modeling parameters of the initial rupture model are given in Table 3. It is seen that the shape of accelerogram at any station is significantly affected by the position of finite fault and nucleation point, dip, strike velocity of the rupture plane. Once the initial position of finite fault has been fixed in the vicinity of the focus, it has been changed iteratively to obtain minimum error position. Table 4 gives the range of the model parameters which are used in the simulation and help in deciding the selecting final rupture model.

Table 3 Modeling parameters for simulation

Modeling parameter	Source
Length—144 km	Wells and Coppersmith (1994)
Width = 40 km	Wells and Coppersmith (1994)
Dip = 6°	CMT Harward
Strike = 287°	CMT Harward
Depth= 12 km	CMT Harward
NL = 3	Kanamori and Aderson (1975)
NW=3	Kanamori and Aderson (1975)
Vr = 2.9 km/s	Fan and Shearer (2015)
β = 3.6 km/s	
$Q\beta(f) = 167f^{0.47}$	Nath and Thingbaijam (2009)

Table 4 Velocity model used to model the Nepal Earthquake, Yu et al. (1995)

Thickness (km)	V_s (km/s)	Density (g/cm^3)
0.4	2.00	1.8
1.0	2.86	2.4
15.0	2.97	2.6
30.0	3.43	2.9

The radiation pattern and the arrival time of the envelope at the observation point are dependent on the position of the rupture plane. To select the final position of the rupture plane, nine different models are checked in a range of + 5 km to − 5 km along dip and strike of the rupture plane. Other parameters of this rupture model are same as that given in Table 3 .Velocity model used in this study are given in Table 4 which was given by Yu et al. (1995). Position of the rupture plane that is considered for simulation at Kantipath station is shown in Fig. 7. Modeled records at Kantipath station for various positions of rupture plane are shown in Fig. 7.

All sub-faults enclosed in the rupture plane have equal possibilities having the starting point of the rupture. The rupture model of Nepal earthquake consists of nine sub-faults, therefore, giving rise to nine possibilities of nucleation point. Acceleration waveform obtained from each possibility is compared with the observed data to get the

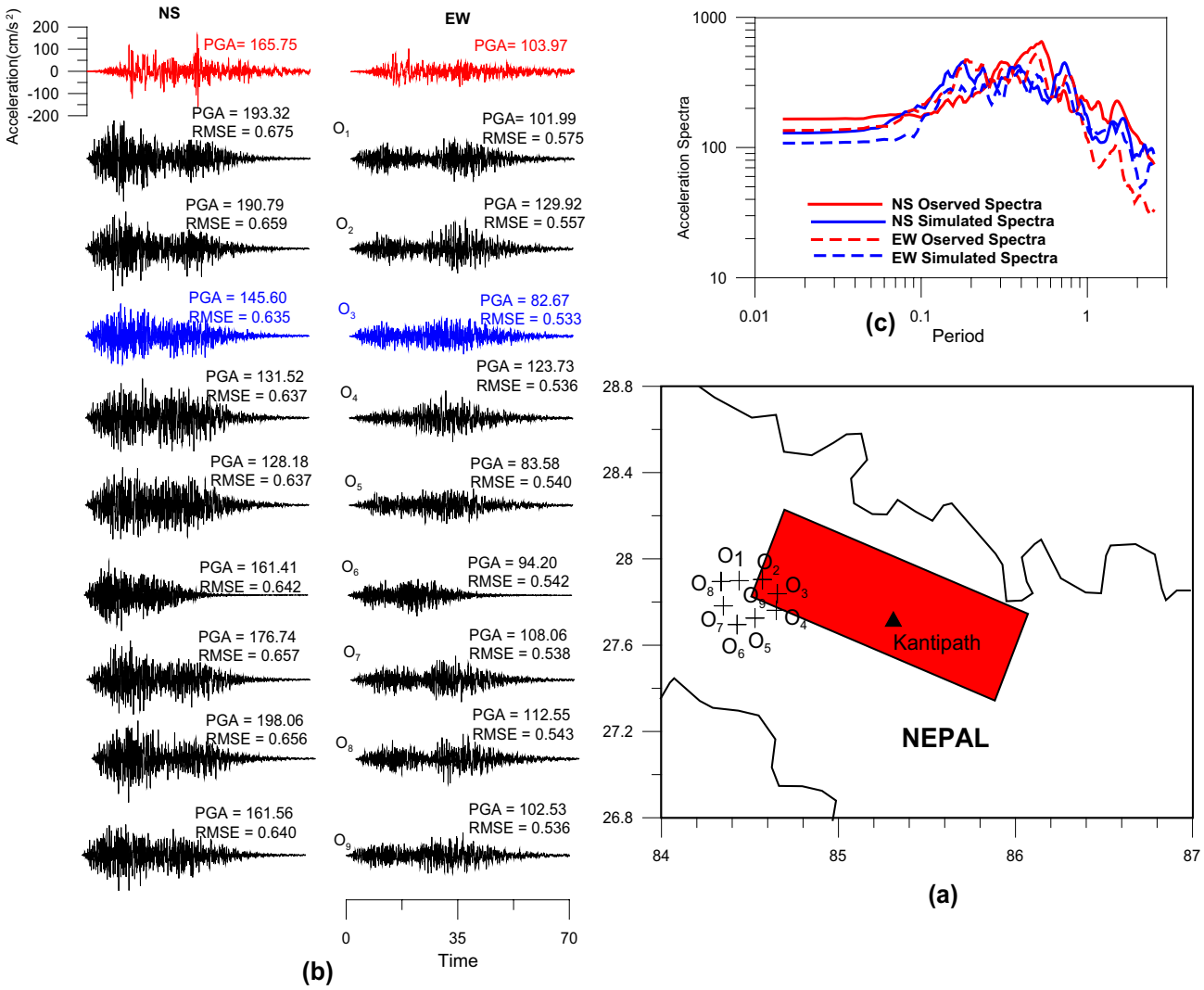

Fig. 7 **a** Various positions at which rupture plane is placed to simulate record at Kantipath Station. **b** Red color shows the observed records, blue color shows the simulated record for rupture positioned O_3 and black color shows the simulated records corresponding to their positions as shown. **c** Comparison of response spectra of simulated record by placing rupture at O_3 with that from observed record

best fit. Minimum RMSE is obtained for the sub-fault located at central element in topmost row acts as nucleation point from Fig. 8.

The rupture velocity is also a controlling factor in the entire simulation process. This affects the arrival time of envelope at the observation point. The initial rupture velocity has been assumed as 2.9 km/s given by Fan and Shearer (2015) and then changing from 2.4 to 3.6 km/s with incremental of 0.2 km/s to get the final rupture velocity.

Seven records were simulated at Kantipath station using range 2.4–3.6 km/s of the velocity of the rupture plane as shown in Fig. 9. The rupture velocity is 3.0 km/s at which the minimum root mean square error has been obtained between the simulated and observed records.

The range of the dip and strike is shown in Table 5. Simulation have been done by changing the dip and strike (range given in Table 5) but no significant changes observe in the rupture parameters, no significant effect on the simulated records and there is no change in the root mean square error between the simulated and recorded record. So the value of the dip and strike used in the present study as given in Table 3.

Simulation of strong ground motion

Once the modeling parameters of the rupture plane are decided, then simulation of the accelerograms at the far field five stations in Kumaon array has been done. These modeled records are compared in terms of its parameters and complete waveform with the observed record. Simulated records do not contain site amplification terms, so the

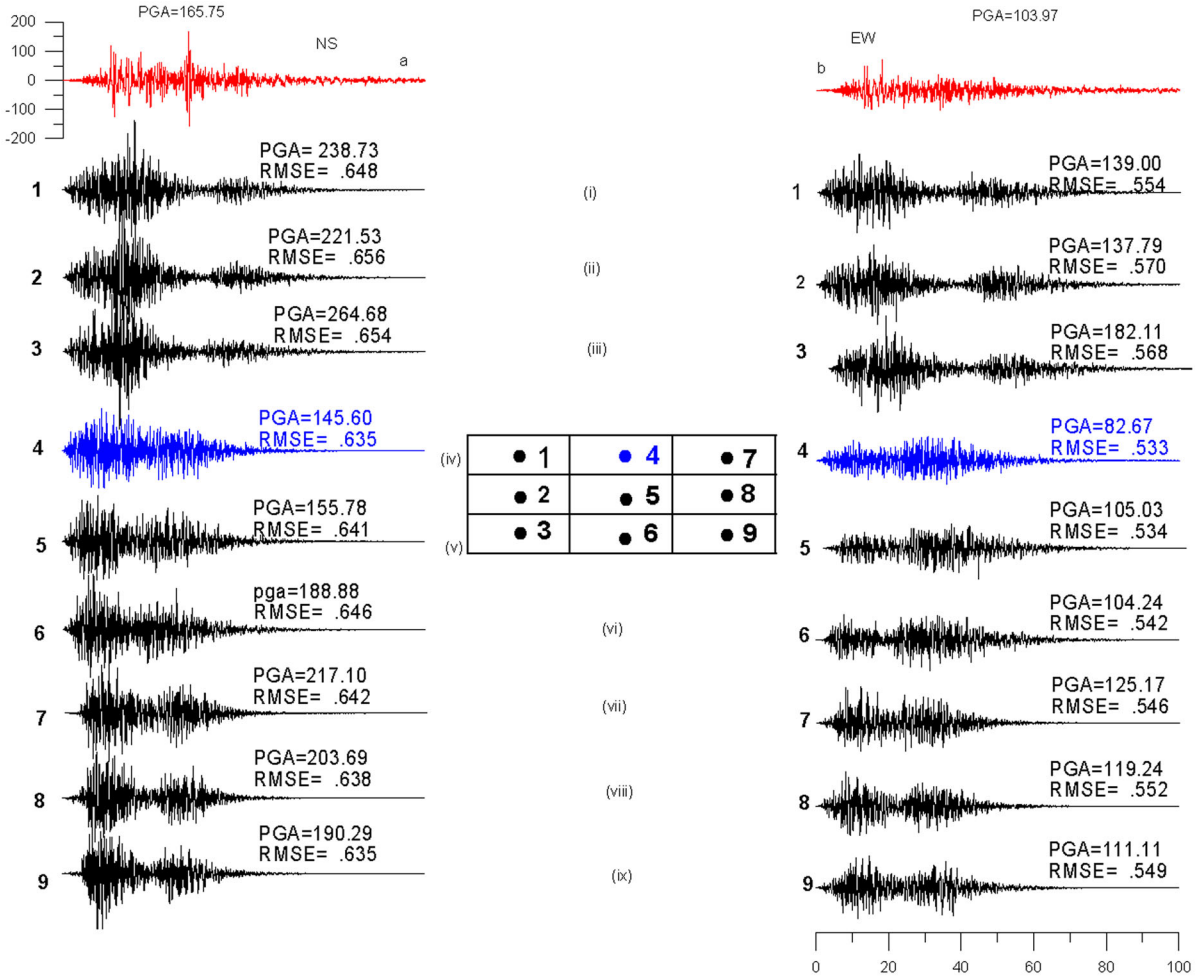

Fig. 8 (i)–(ix) gives simulated NS and EW component for the nucleation point from 1 to 9 at Kantipath station. Blue record represents minimum root mean square error between simulated and observed waveform

observed records need to be corrected for hard rock. So it is required to remove the site effect from the recorded records at each station. The simulation technique used in the present study uses quality factor $Q_\beta(f)$ of S wave. Quality factor $Q_\beta(f)$ of S wave is used at different four stations as given in Table 6 (Joshi et al. 2012c). As Kapkot station has no more sufficient data to calculate the quality factor of shear wave. The observed records at hard rock site after correcting the soil amplification have been simulated at Kapkot station using nearby $Q_\beta(f)$ obtained at Bagehswar station which lies at a distance of 17 km. Observed and simulated records at rock site are compared and shown in Fig. 10 and Fig. 11 shows the comparision between the response spectra of the observed and simulated records. Comparision of the PGA of the observed and simulated for the NS and EW components are shown in Fig. 12. PGA at hard rock site obtained from modeled record and processed observed record is shown in Table 7 with epicentral distance.

The corrected S phase portion is used for comparing the observed and modeled records and best fit in terms of its statistical parameters and shape. The response spectra of the simulated record between time period 0.2–2 s are comparable with the observed response spectra in the same interval and the response spectra have been determined at 5% damping.

Station wise simulation

Kanalichina

The simulated accelerogram is comparable with the observed accelerogram in terms of statistical parameters and shape. The response spectrum of synthetic records matches with that response spectra of observed records. Peak ground acceleration of the observed and simulated time series are comparable for both horizontal components.

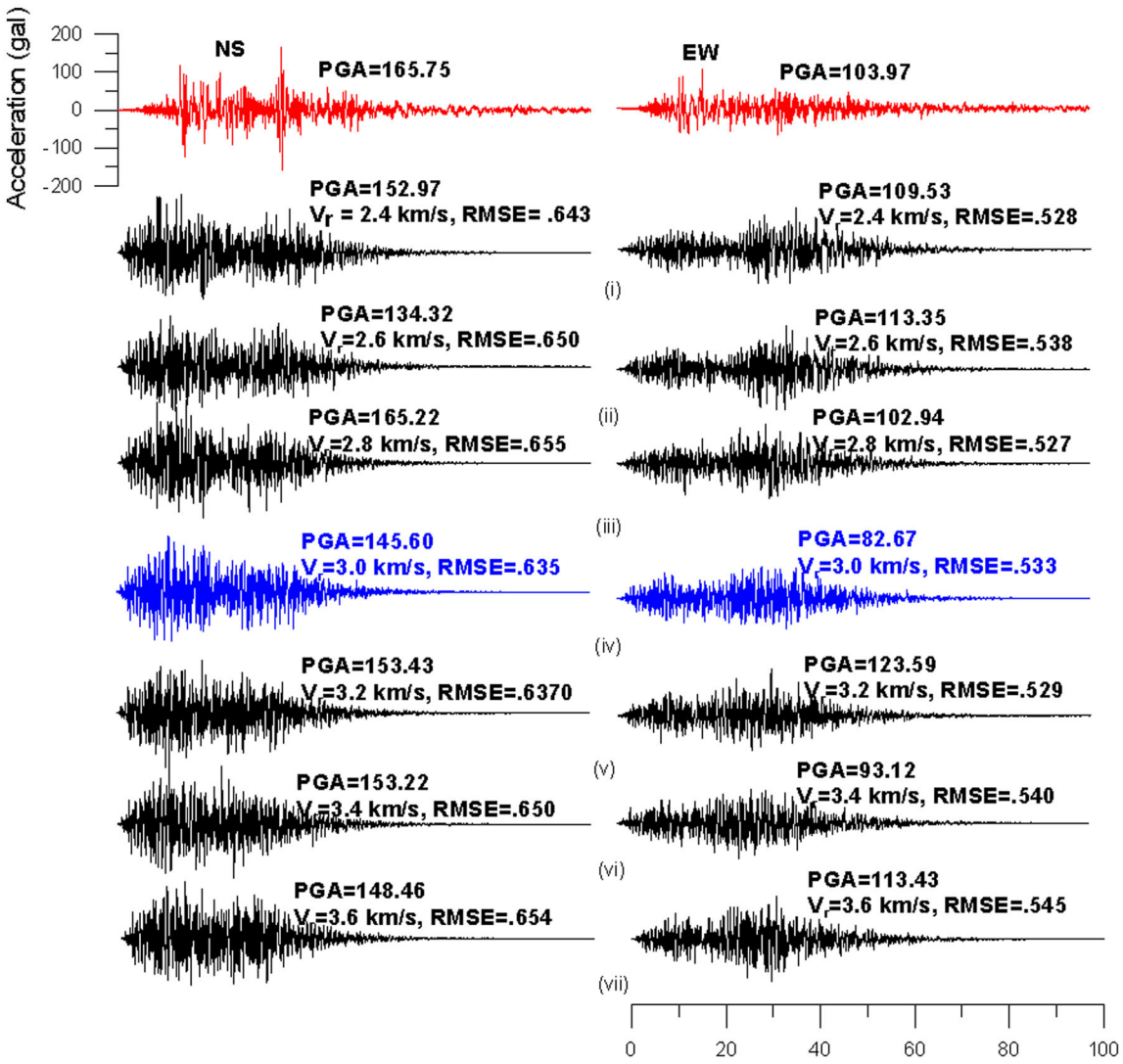

Fig. 9 The simulated NS and EW component for rupture velocity from 2.4 to 3.6 is shown in (i) to (vii), respectively, at Kantipath

Table 5 Range of modeling parameters

Model parameter	Range
Location	Several possible locations in all direction at a uniform distance of 5 km
Starting point of rupture	All elements
Rupture velocity *Vr*	2.4–3.6 km/s
Dip	2–10°
Strike	282–292°

Bageshwar

The simulated accelerogram is comparable with the observed accelerogram in terms of statistical parameters and shape. The response spectrum of synthetic records matches with that response spectra of observed records. Peak ground acceleration of the observed and simulated time series are comparable for both horizontal components.

Berinag

The simulated accelerogram is comparable with the observed accelerogram in terms of statistical parameters and shape. The comparison is based on the root mean square error between the observed and simulated records. The response spectrum of synthetic records matches with response spectra of observed records. Peak ground acceleration of the observed and simulated time series are comparable for both horizontal components.

Table 6 Q relations for stations of the Kumaon Himalaya except Kapkot (Joshi et al. 2012c)

Stations	Obtained result for NS component		Obtained result for EW component		Final $Q_\beta(f)$ relation using value of $Q_\beta(f)$ obtained from NS and EW component separately
	$Q_\beta(f)$ relation	RMSE	$Q_\beta(f)$ relation	RMSE	$Q_\beta(f)$ relation
Bhageshwar	$(34 \pm 4.1)f^{(1.2 \pm 0.10)}$	0.0328	$(41 \pm 5.1)f^{(1.2 \pm 0.12)}$	0.0212	$(39 \pm 4.7)f^{(1.2 \pm 0.11)}$
Berinag	$(15 \pm 2.1)f^{(1.3 \pm 0.15)}$	0.0566	$(23 \pm 2.2)f^{(1.2 \pm 0.09)}$	0.0360	$(21 \pm 5.7)f^{(1.2 \pm 0.11)}$
Knalichhina	$(22 \pm 2.9)f^{(1.3 \pm 0.10)}$	0.0682	$(19 \pm 2.9)f^{(1.4 \pm 0.12)}$	0.0572	$(22 \pm 3.0)f^{(1.3 \pm 0.09)}$
Kamedidevi	$(27 \pm 4.4)f^{(1.0 \pm 0.09)}$	0.0863	$(24 \pm 4.2)f^{(0.9 \pm 0.07)}$	0.0783	$(25 \pm 5.4)f^{(0.9 \pm 0.06)}$

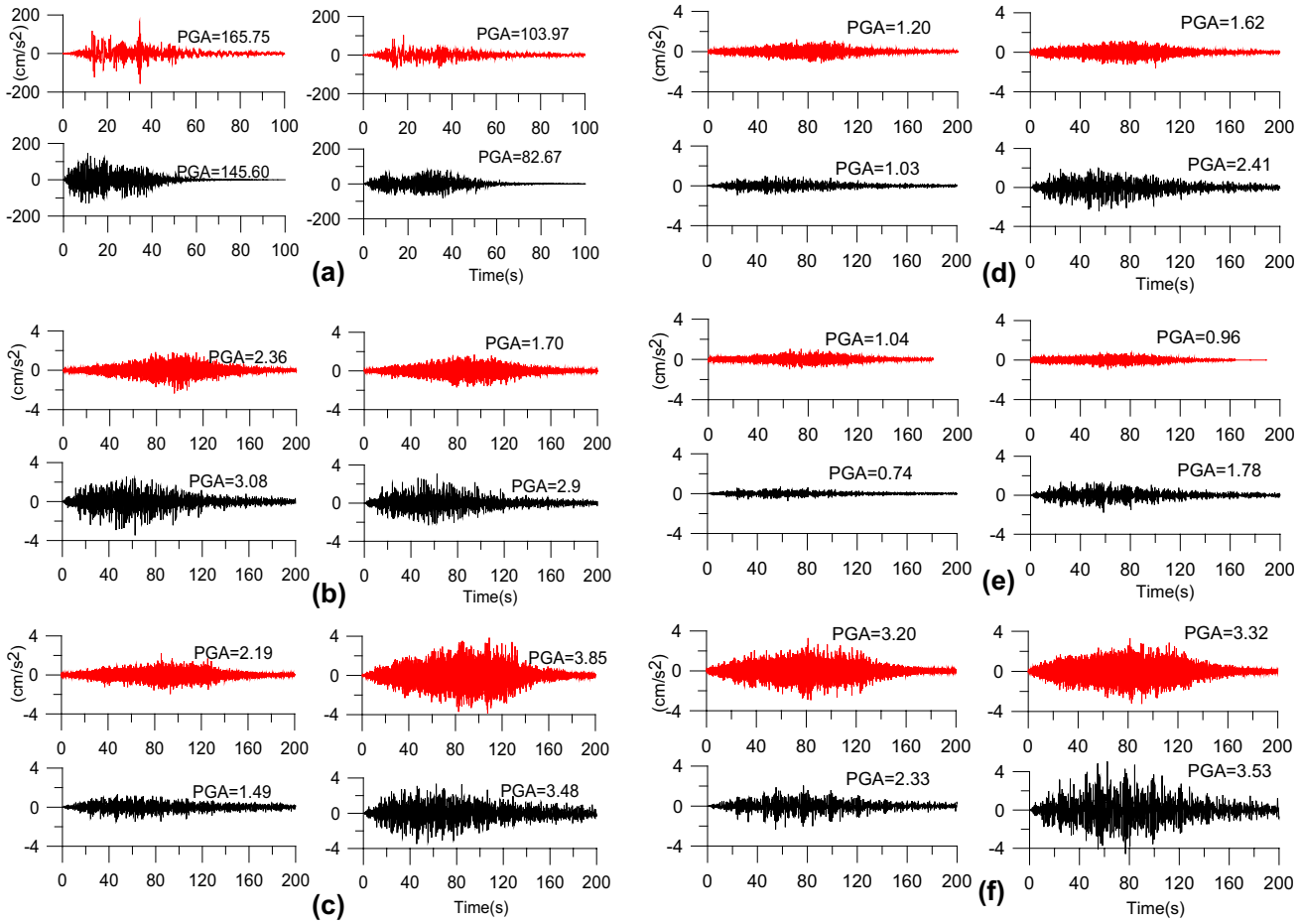

Fig. 10 Both the time histories of the north south and east west components for observed and simulated records are compared at. **a** Kantipath, **b** Knalichina, **c** Bageshwar, **d** Berinag, **e** Kamedidevi, **f** Kapkot .Red color represents the observed records and black color represents the simulated records, respectively

Kamedidevi

The simulated accelerogram is comparable with the observed accelerogram in terms of statistical parameters and shape. The comparison is based on the root mean square error between the observed and simulated records. The response spectrum of synthetic records matches with that response spectra of observed records. Peak ground acceleration of the observed and simulated time series are comparable for both horizontal components.

Kapkot

The simulated accelerogram is comparable with the observed accelerogram in terms of statistical parameters and shape. The comparison is based on the root mean

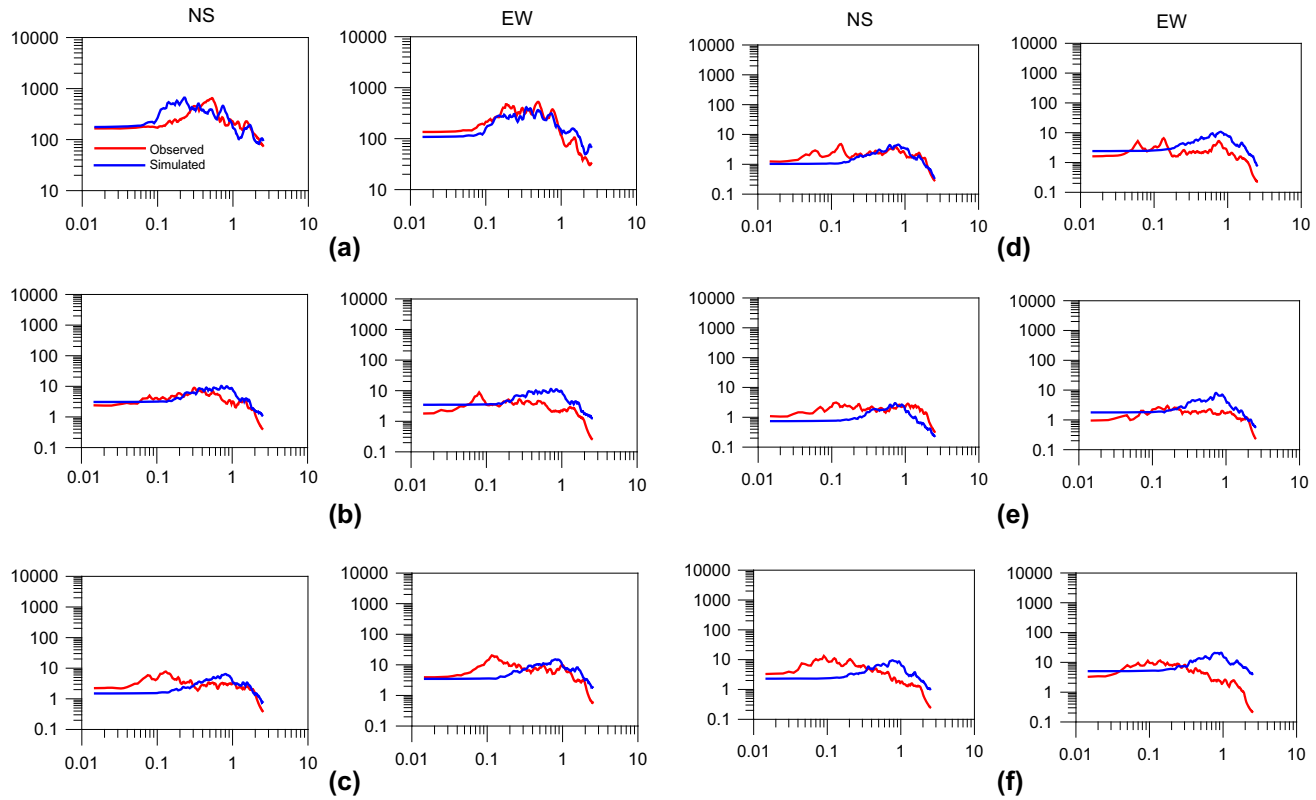

Fig. 11 Responses spectra which are obtained from simulated time series and observed time series of NS and EW components are compared in a reasonable range at. **a** Kantipath, **b** Knalichina, **c** Bageshwar, **d** Berinag, **e** Kamedidevi, **f** Kapkot. Red color represents the observed records spectra and black color represents the simulated records spectra, respectively

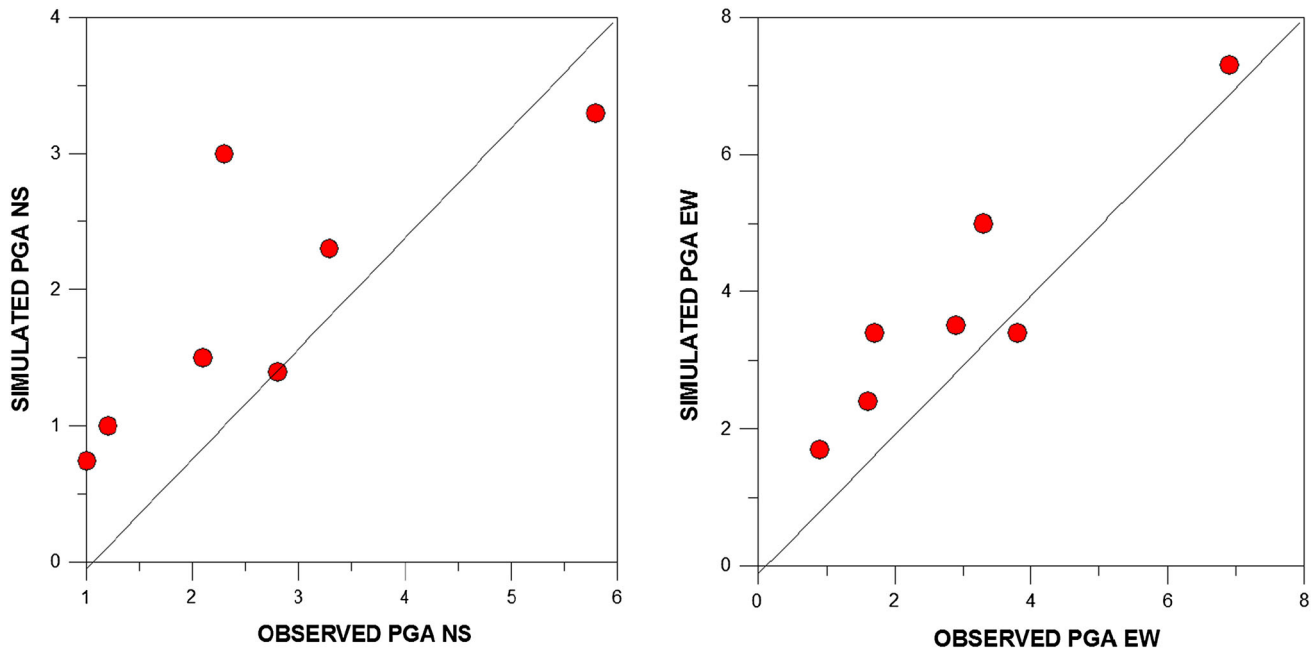

Fig. 12 Comparison between the simulated PGA and observed PGA for the NS and EW components, respectively

square error between the observed and simulated records. The response spectrum of synthetic records matches with that response spectra of observed records. The reason for that $Q_\beta(f)$ for this region is not sufficient to provide good

Table 7 Maximum PGA of the observed and simulated records with epicentral distance from the epicenter of the Earthquake

Sr. no.	Stations	Epicentral distance (km)	PGA obtained from NS component	PGA obtained from EW component	PGA simulated from NS component	PGA simulated from EW component
1	Knalichina	463.6	2.36	1.70	3.08	3.46
2	Bageshwar	515.1	2.19	3.85	1.49	3.48
3	Berinag	487.4	1.20	1.62	1.03	2.41
4	Kamedidevi	498.3	1.04	0.96	0.74	1.78
5	Kapkot	508.6	3.20	3.32	2.33	3.53

matching. A comparable best fit between peak ground acceleration of NS and EW is simulated and the observed data have been observed. The Q relations for all stations of the Kumaon Himalaya array are given in Table 6 except the Kapkot due to non-availability of the data.

Conclusions

We had used strong motion data of the Nepal main shock ($M_w = 7.9$) and aftershock ($M_w = 6.6$) to model the Nepal main shock which were recorded on far field station installed in Kumaon Himalaya region. Strong motion data of the aftershock are used to determine the source parameters of the aftershock which is used to model the Nepal main shock. The average value of the seismic moment and stress drop is 8.26×10^{25} dyn cm and 10.48 bar, respectively, for the aftershock. Initially near field strong motion data recorded at Kantipath station is modeled by changing the nucleation point, rupture velocity several possible location and then finalized the parameters based on the root mean square between the observed and simulated records and their response spectra. It is concluded that changing location, nucleation point and rupture velocity has more affect the modeled time series. These final parameters are used to model the far field strong motion data recorded at stations in Kumaon Himalaya.

The comparison of full waveform and its response spectra has been made to finalize the rupture parameters and its location. The comparison of observed and simulated records shows that this earthquake was triggered by a rupture propagating in NE–SW direction with a rupture velocity 3.0 km/s from a distance of 80 km from Kathmandu at a depth of 12 km. Simulation of the strong motion due to an earthquake is widely used in the earthquake engineering other branches of the engineering seismology. The simulation of the Nepal earthquake is helpful in estimating the seismic hazard assessment and to understand the source modeling of the earthquake.

Acknowledgements The authors would like to express deep sense of gratitude and sincere indebtedness to Indian Institute of Technology, Roorkee for supporting this research work and very thankful to MOES, Government of India granting from Grant No. MoES-800-ESD/2014.

References

Aki K (1967) Scaling law of seismic spectrums. J Geophys Res 72:1217–1231

Atkinson GM, Boore DM (1995) Ground motion relations for Eastern North America. Bull Seismol Soc Am 85:17–30

Atkinson GM, Boore DM (1998) Evaluation of models for earthquakes source spectra in Eastern North America. Bull Seismol Soc Am 88:917–934

Atkinson GM, Boore DM (2006) Earthquake ground-motion prediction equations for Eastern North America. Bull Seism Soc Am 96(6):2181–2205

Beresnev IA, Atkinson GM (1997) Modeling finite-fault radiation from the omega-n spectrum. Bull Seismol Soc Am 87:67–84

Beresnev IA, Atkinson GM (1999) Generic finite-fault model for ground-motion prediction in eastern North America. Bull Seism Soc Am 89:608–625

Boore DM (1983) Stochastic simulation of high frequency ground motions based on seismological models of the radiated spectra. Bull Seismol Soc Am 73:1865–1894

Boore DM, Bommer JJ (2005) Processing of strong-motion accelerograms: needs, options and consequences. Soil Dyn Earthq Eng 25:93–115

Boore DM, Joyner WB (1991) Estimation of ground motion at deep soil sites Eastern North America. Bull Seismol Soc Am 81:2167–2185

Brune JN (1970) Tectonic stress and spectra of seismic shear waves from earthquakes. J Geophys Res 75:4997–5009

CEDIM Report 3: Nepal Earthquakes (2015). CEDIM forensic disaster analysis group, CATDAT and Earthquake-Report.com

Fan Wenyuan, Shearer Peter M (2015) Detailed rupture imaging of the 25 April 2015 Nepal earthquake using teleseismic P waves. Geophys Res Lett 42:5744–5752

Frankel A (1991) High–frequency spectral falloff of earthquakes, fractal dimension of complex rupture, b value, and scaling of strength on faults. J Geophys Res 96:6291–6302

Fukuyama E, Irikura K (1986) Rupture process of the 1983 Japan sea (Akita-Oki) earthquake using a waveform inversion method. Bull Seism Soc Am 76:1623–1640

Haddon RAW (1996) Use of empirical green's functions, spectral ratios, and kinematic source models for simulating ground motion. Bull Seismol Soc Am 86:597–615

Hadley DM, Helmberger DV, Orcutt JA (1982) Peak acceleration scaling studies. Bull Seism Soc Am 72:959–979
Hanks TC, McGuire RK (1981) The character of high frequency ground motion. Bull Seism Soc Am 71:2071–2095
Hartzell SH (1978) Earthquake aftershocks as Green's functions. Geophys Res Let 5:1–4
Hartzell SH (1982) Simulation of ground accelerations for May 1980 Mammoth Lakes, California earthquakes. Bull Seism Soc Am 72:2381–2387
Heaton TH, Hartzell SH (1989) Estimation of strong ground motions from hypothetical earthquakes on the Cascadia subduction zone, Pacific Northwest. Pure Appl Geophys 129:131–201
Housner GW, Jennings PC (1964) Generation of artificial earthquakes. Proc ASCE 90:113–150
Houston H, Kanamori H (1984) The effect of asperities on short period seismic radiation with application on rupture process and strong motion. Bull Seism Soc Am 76:19–42
Hutchings L (1985) Modelling earthquakes with empirical Green's functions (abs). Earthquake Notes 56:14
Imagawa K, Mikami N, Mikumo T (1984) Analytical and semi empirical synthesis of near-field seismic waveforms for investigating the rupture mechanism of major earthquakes. J Physics of Earth 32:317–338
Irikura K (1983) Semi empirical estimation of strong ground motion during large earthquakes. Bull Dis Prevent Res Inst 33:63–104
Irikura K, Kamae K (1994) Estimation of strong ground motion in broad–frequency band based on a seismic source scaling model and an Empirical Green's function technique. Ann Geofis XXXVII 6:1721–1743
Irikura K, Kagawa T, Sekiguchi H (1997) Revision of the empirical Green's function method by Irikura 1986. Programme and abstracts. Seismol Soc Jpn 2:B25
Joshi A (2004) A simplified technique for simulating wide band strong ground motion for two recent Himalaya earthquakes. Pure Appl Geophys 161:1777–1805
Joshi A, Midorikawa S (2004) A simplified method for simulation of strong ground motion using rupture model of the earthquake source. J Seismol 8:467–484
Joshi A, Patel RC (1997) Modelling of active lineaments for predicting a possible earthquake scenario around Dehradun, Garhwal Himalaya, India. Tectonophysics 283:289–310
Joshi A, Sandeep, Kamal (2014) Modelling of strong motion generation areas of the 2011 Tohoku, Japan earthquake using modified semi empirical technique. Nat Hazards 71:587–609
Joshi A, Kumar B, Sinvhal A, Sinvhal H (1999) Generation of synthetic accelerograms by modelling of rupture plane. J earthq Technol 36:43–60
Joshi A, Singh S, Giroti K (2001) The Simulation of ground motions using envelope summations. Pure Appl Geophys 158:877–901
Joshi A, Kumari P, Sharma ML, Ghosh AK, Agarwal MK, Ravikiran A (2012a) A strong motion model of the 2004 great Sumatra earthquake: simulation using a modified semi empirical method. J Earthq Tsunami 6:1–29
Joshi A, Kumari P, Singh S, Sharma ML (2012b) Near–field and far–field simulation of accelerograms of Sikkim earthquake of September 18, 2011 using modified semi empirical approach. Nat Hazards 64:1029–1054
Joshi A, Kumar P, Mohanty M, Bansal AR, Dimri VP, Chadha RK (2012c) Determination of $Q_\beta(f)$ in different parts of Kumaon Himalaya from the inversion of spectral acceleration data. Pure Appl Geophys 169:1821–1845
Joshi A, Tomer Monu, Lal Sohan, Chopra Sumer, Singh Sandeep, Sanjay Parjapati ML, Sharma Sandeep (2016) Estimation of source parameters of Nepal earthquake from strong motion data. Nat Hazards 83:867–883
Kameda H, Sugito M (1978) Prediction of strong earthquake motions by evolutionary process model. In: Proceedings of the sixth Japan earthquake engineering symposium, pp 41–48
Kanamori H (1979) A semi empirical approach to prediction of long period ground motions from great earthquakes. Bull Seism Soc Am 69:1645–1670
Kanamori H, Anderson DL (1975) Theoretical basis of some empirical relations in seismology. Bull Seism Soc Am 65:1073–1095
Khattri KN (1987) Great earthquakes, seismicity gaps and potential for earthquake disaster along the Himalayan Plate boundary. Tectonophysics 138:79–92
Khattri KN, Zeng Y, Anderson JG, Brune J (1994) Inversion of strong motion waveforms for source slip function of 1991 Uttarkashi earthquake, Himalaya. J Himalayan Geol 5:163–191
Kohrs-Sansorny C, Courboulex F, Bour M, Deschamps A (2005) A two-stage method for ground-motion simulation using stochastic summation of small earthquakes. Bull Seismol Soc Am 84:31–46
Kumar D, Sarkar I, Sriram V, Khattri KN (2005) Estimation of the source parameters of the Himalaya earthquake of October 19, 1991, average effective shear wave attenuation parameters and local site effects from accelerograms. Tectonophysics 407:1–24
Lai SP (1982) Statistical characterization of strong motions using power spectral density. Bull Seismol Soc Am 72:259–274
McGuire RK, Becker AM, Donovan NC (1984) Spectral estimates of shear waves. Bull Seismol Soc Am 74:2167–2185
Midorikawa S (1993) Semi empirical estimation of peak ground acceleration from large earthquakes. Tectonophysics 218:287–295
Munguia L, Brune JM (1984) Simulations of strong ground motions for earthquakes in the Mexicali–Imperial Valley. In: Proc. of workshop on strong ground motion simulation and earthquake engineering applications, Pub. 85–02. Earthquake Engineering Research Institute, Los Altos, CA 21–1–21–19
Nakamura Y (1989) A method for dynamic characteristics estimation of subsurface using microtremor on the ground surface. Quarterly Report of RTRI 30:1, pp 25–33
Nath SK, Thingbaijam KKS (2009) Seismic Hazard assessment—a holistic microzonation approach. Nat Hazards Earth Syst Sci 9:1445–1495
Safarshahi M, Rezapour M, Hamzehloo H (2013) Stochastic finite-fault modelling of ground motion for the 2010 Rigan earthquake, Southeastern Iran. Bull Seism Soc Am 103(1):223–235
Sinozuka M, Sato Y (1967) Simulation of non stationary random processes. Proc. ASCE 93:11–40
Sriram V, Khattri KN (1997) A study of source spectrum, site amplifications, response spectra, Fourier Spectra and peak ground accelerations from the strong ground motion data of the Uttarkashi earthquake. Curr Sci 72:728–740
Wason HR, Sharma ML (2000) Source parameters study of local earthquakes in the Garhwal Himalaya region based on the digital broad band data. In: 12th World conference on earthquake engineering; Auckland, New Zealand, Sunday 30 January–Friday 4 February 2000, paper—1776
Wells DL, Coppersmith KJ (1994) New empirical relationships among Magnitude, Rupture Length, Rupture width, Rupture Area, and source displacement. Bull Seismol Soc Am 84:974–1002
Yin A (2006) Cenozoic tectonic evolution of the Himalayan orogen as constrained by along-strike variation of structural geometry, exhumation history, and forehand sedimentation. Earth Sci Rev 76:1–131
Yu G (1994) Some aspects of earthquake Seismogy: slip partitioning along major convergent plate boundaries; composite source

model for estimation of strong motion; and nonlinear soil response modelling. PhD thesis, University of Nevada

Yu G, Khattri KN, Anderson JG, Brune JN, Zeng Y (1995) Strong ground motion from the Uttarkashi, Himalaya, India, earthquake: comparison of observations with synthetics using the composite source model. Bull Seism Soc Am 85:31–50

Zeng Y, Anderson JG, Su F (1994) A composite source model for computing realistic synthetic strong ground motions. Geophys Res Let 21:725–728

Websites used

http://www.globalcmt.org/CMTsearch.html.
https://earthquake.usgs.gov/.